Note

Feng-Yang Hsieh

1 CWoLa

The Classification Without Labels (CWoLa) is a weakly supervised learning method. The CWoLa approach trains a model to discriminate the mixed samples, which are mixtures of the original signal and background samples. The optimal classifier in the CWoLa approach is also the optimal classifier in the traditional fully supervised case where all label information is available. This section utilizes the CWoLa approach to train classifiers on di-Higgs samples.

1.1 Sample

This exercise's signal corresponds to the resonant Higgs boson pairs production in the four-b quarks channel. These Higgs boson pairs are produced via gluon-gluon fusion in the two Higgs doublet model (2HDM). The Higgs boson h ($m_h = 125$ GeV) pair is produced by the heavy CP-even scalar H with mass m_H ranging from 300 GeV to 1200 GeV. The background consists of QCD multi-jet events.

The CWoLa training samples M_1 and M_2 are the mixtures of the signal and background samples. The probability distribution of the mixed sample is a combination of the signal $p_s(x)$ and background $p_B(x)$ distributions:

$$\begin{aligned} p_{M_1}(x) &= f_1 p_S(x) + (1 - f_1) p_B(x) \\ p_{M_2}(x) &= f_2 p_S(x) + (1 - f_2) p_B(x) \end{aligned} \tag{1}$$

where f_1, f_2 are the signal fractions, and x represents the observables used for the classification task.

DNN and SPANet network architectures are considered in this exercise. For DNN, the input features are summarised in Table 1, consisting of 16 variables. For SPANet, the input features are a list of final jets, each represented by their 4-momentum $(p_{\mathrm{T}}, \eta, \phi, M)$ and a boolean b-tag.

Table 1: Input variables used to train the dense neural network.

Reconstructed objects	Variables used for training	#
Higgs candidate	$(p_{\mathrm{T}}, \eta, \phi, m)$	8
Subjets	$\Delta R(j_1, j_2)$	2
b-tagging	Boolean for $j_i \in h_{1,2}^{\mathrm{cand}}$	4
Di-Higgs system	$p_{\mathrm{T}}^{hh}, m_{hh}$	2

1.2 Result

The CWoLa training utilizes samples with different signal fractions f_1, f_2 to train the classifiers. The results of CWoLa training are shown in Figure 1 with different signal fractions. When f_1 is far from 0.5, the results tend to approach those of the fully supervised case.

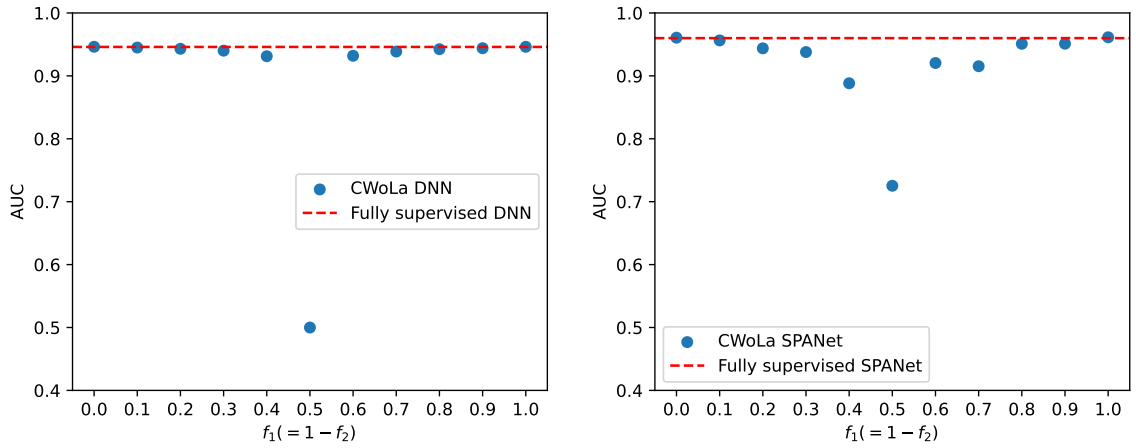

(a) DNN (b) SPANet

Figure 1: The AUC of CWoLa training as a function of the signal fraction f_1. For simplicity, we set signal fraction f_2 equal to $1 - f_1$. The horizontal dashed line indicates the fully-supervised AUC.

When $f_1 = 0.5$ the mixed sample M_1 and M_2 have identical distributions, so the classifier can not learn anything in this case. In the case of DNN, the AUC is 0.5, as expected. However, for SPANet, the AUC is more than 0.7.

This is because SPANet is trained on both pairing and classification tasks simultaneously. The pairing part introduces asymmetries between signal and background samples, leading to the AUC that deviates from 0.5.

To investigate the effect of the pairing task on SPANet's performance, the weight of the

pairing component is set to zero, meaning that SPANet focuses solely on the classification task. Figure 2 shows the SPANet training results without pairing task. As expected, the AUC is close to 0.5 when $f_1 = 0.5$.

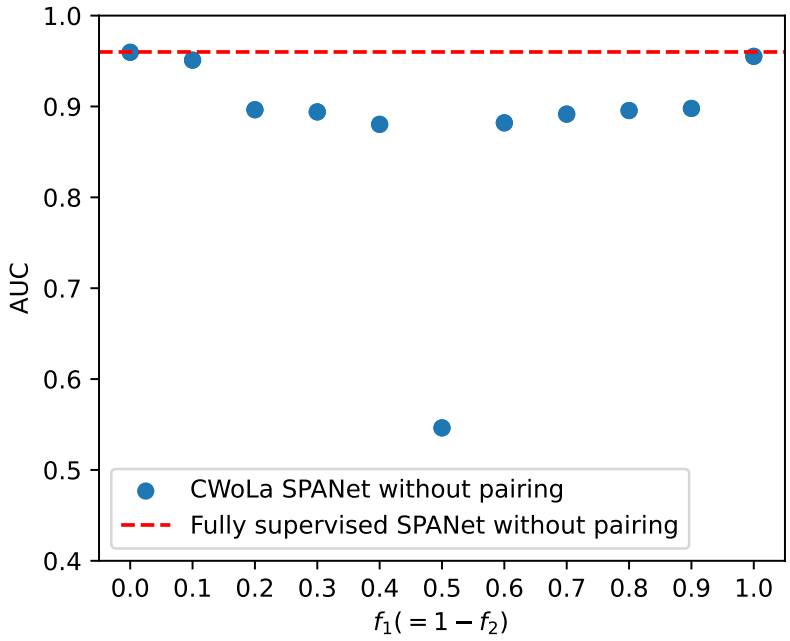

Figure 2: The AUC of CWoLa SPANet training as a function of the signal fraction f_1. For simplicity, we set signal fraction f_2 equal to $1 - f_1$. Here, SPANet is trained on the classification task only.

2 CWoLa hunting

The CWoLa hunting approach considers a variable m_{res}. For background, the m_{res} distribution is smooth while signal m_{res} distribution is expected to be localized near some m_0. Consequently, this variable could be used to create two mixed samples. Additional features that are uncorrelated with m_{res} can be used for training a classifier. This technic is first introduced by Reference [1].

2.1 Sample

The signal is the resonant Higgs boson pairs production in the four-b quarks channel. In this section, the Higgs boson pair is produced by the heavy CP-even scalar H with mass $m_H = 500$ GeV or $m_H = 1000$ GeV. The background consists of QCD multi-jet events. The

basic requirement is the "four-tag cut," which requires at least four b-tagged $R = 0.4$ anti-k_t jets with $p_{\mathrm{T}} > 40$ GeV and $|\eta| < 2.5$. Only the events passing the four-tag cut are used in the following analysis.

The CWoLa hunting approach utilizes the signal and sideband regions to create the mixed training sample. The di-Higgs system's total invariant mass m_{hh} is utilized to determine the signal and sideband region. This quantity is computed from the four b-jets with the highest transverse momentum. Figure 3 presents the m_{hh} distribution of signal and background samples. Table 2 summarizes the signal and sideband regions. These signal and sideband regions are chosen such that the corresponding cross-sections are closed.

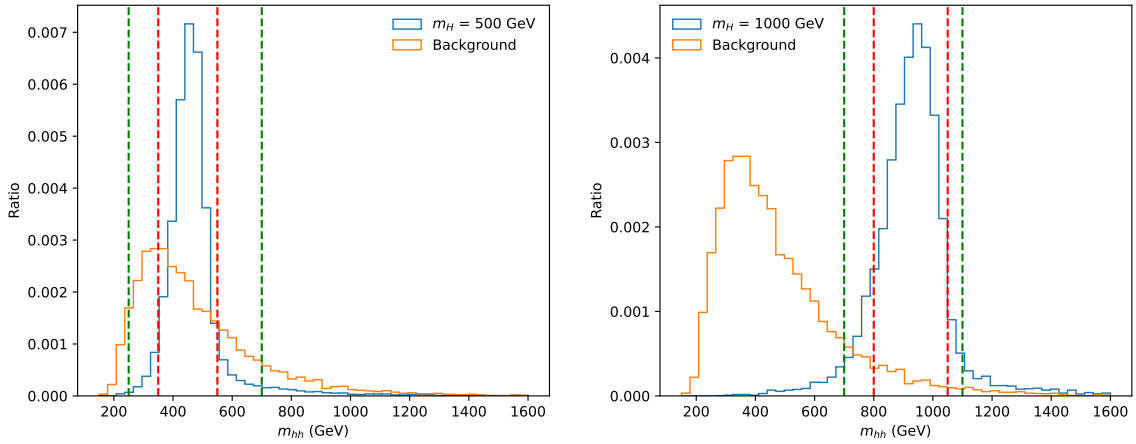

(a) $m_H = 500$ GeV (b) $m_H = 1000$ GeV

Figure 3: The total invariant mass m_{hh} distribution of signal and background samples. The signal region is between the red dashed lines. The sideband region is between the green dashed lines and excludes the signal region.

Table 2: The signal and sideband regions with different resonant samples. The unit is GeV.

m_H	Signal	Sideband
500	$[350, 550]$	$[250, 350] \cup [550, 700]$
1000	$[800, 1050]$	$[700, 800] \cup [1050, 1100]$

Table 3 is the cutflow table of the selection cuts. The number of events used in mixed training samples could be computed from these cross-sections. The training sample size is presented in Table 4.

Consider the DNN CWoLa classifier. The Higgs candidates are reconstructed by the min-ΔR pairing method. In the min-ΔR method, the four b-tagged jets with the highest p_{T}

Table 3: The cross sections for the di-Higgs signal and background processes at different selection cuts.

m_H (GeV)		Cross section (fb) Signal	Background	S/B	$\mathcal{L} = 139$ fb^{-1} $S/\sqrt{B}$
500	Four tag	3.64	6.03e+03	6.03e-04	0.553
	Signal region	3.13	2.57e+03	1.22e-03	0.727
	Sideband region	0.35	2.36e+03	1.50e-04	0.086
1000	Four tag	0.081	6.03e+03	1.34e-05	0.0123
	Signal region	0.063	3.32e+02	1.90e-04	0.0408
	Sideband region	0.010	3.19e+02	3.03e-05	0.0064

Table 4: The training sample size for the mixed sample. The luminosity is $\mathcal{L} = 78$ fb^{-1} because the generated samples are not enough for now.

m_H (GeV)	Mixed sample	True label Signal	Background
500	M_1	244	200k
	M_2	28	184k
1000	M_1	5	26k
	M_2	1	25k

are used to form the two Higgs boson candidates. The min-ΔR method selects the pairing configuration in which the higher-p_{T} jet pair has the smallest ΔR separation. The input features are similar to the previous case (Table 1), but the b-tagging information and the di-Higgs system's total invariant mass are excluded. For min-ΔR pairing, it only uses the b-tagged jets. Total invariant mass is already used to determine the signal and sideband region.

2.2 Training results

Table 5 presents the DNN classification training results. These numbers are evaluated from the pure samples, which consist of 5k signal events and 5k background events. The training datasets with and without signal events have similar results. This suggests that the DNN fails to distinguish the signal and background samples but learns the difference between the signal and sideband region. Moreover, the results also imply the input features may correlate to the total invariant mass of the di-Higgs system.

Table 5: The CWoLa DNN training results. ACC is the best accuracy and AUC is the area under the ROC curve. The average and standard deviation of 10 training are presented.

m_H (GeV)		ACC	AUC
500	With signal	0.708 ± 0.002	0.770 ± 0.007
	No signal	0.705 ± 0.003	0.769 ± 0.009
1000	With signal	0.868 ± 0.024	0.925 ± 0.023
	No signal	0.850 ± 0.033	0.909 ± 0.026

Figure 4 shows the signal score distributions. Even though the signal scores are very different for signal and background distributions, the difference probably stems from the m_{hh} distribution.

There are two issues:

- The input features might correlated to the observables used to determine the signal and sideband region. We need to construct other independent input variables.
- The signal fraction is too low. It is hard to learn something about signal events.

2.3 Correlation matrix

The results in Section 2.2 imply that the di-Higgs system's total invariant mass is not independent of other input features. To find the variables that are highly dependent on

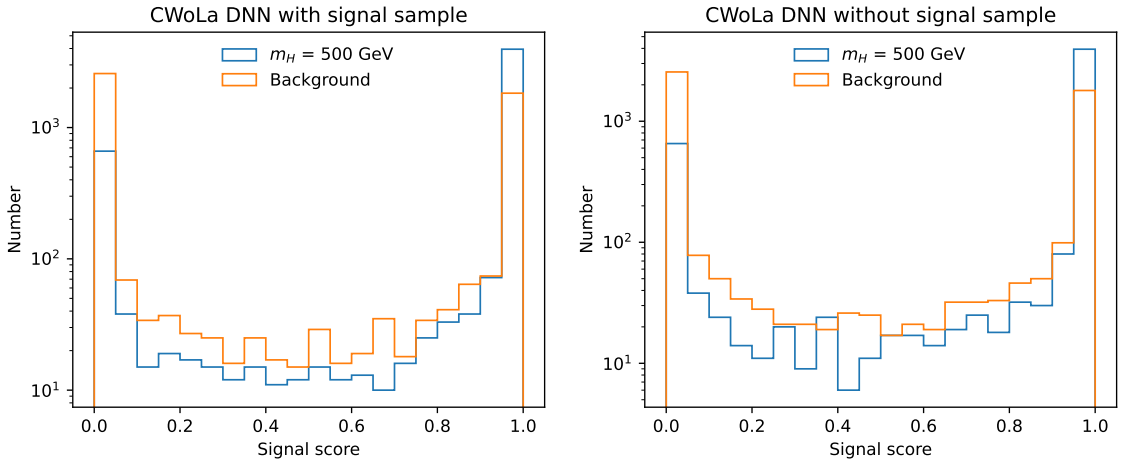

(a) $m_H = 500$ GeV

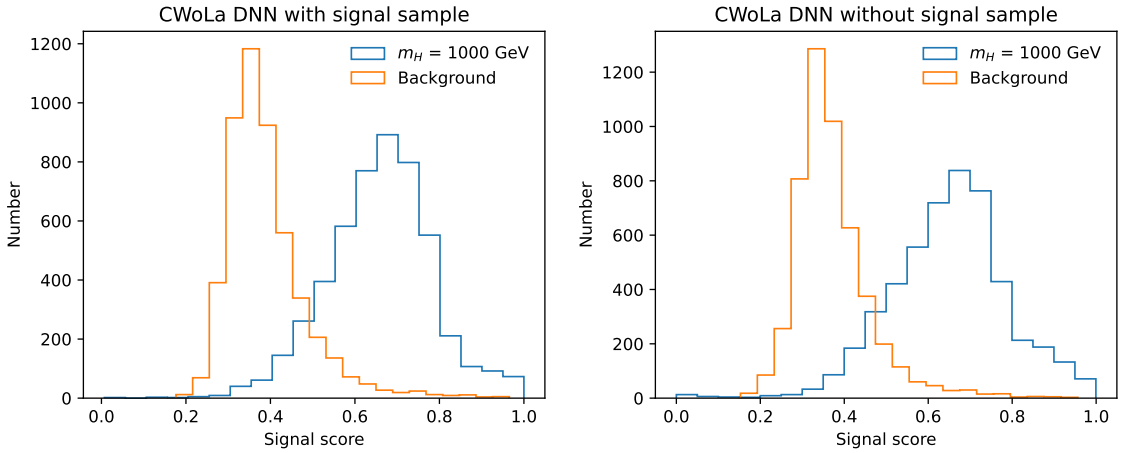

(b) $m_H = 1000$ GeV

Figure 4: The signal score distributions. We apply the CWoLa DNN on pure samples to obtain the signal score distributions.

the total invariant mass, the correlation coefficients are computed among these variables. Figure 5 and 6 are correlation coefficients on the 500 GeV and 1000 GeV cases, respectively.

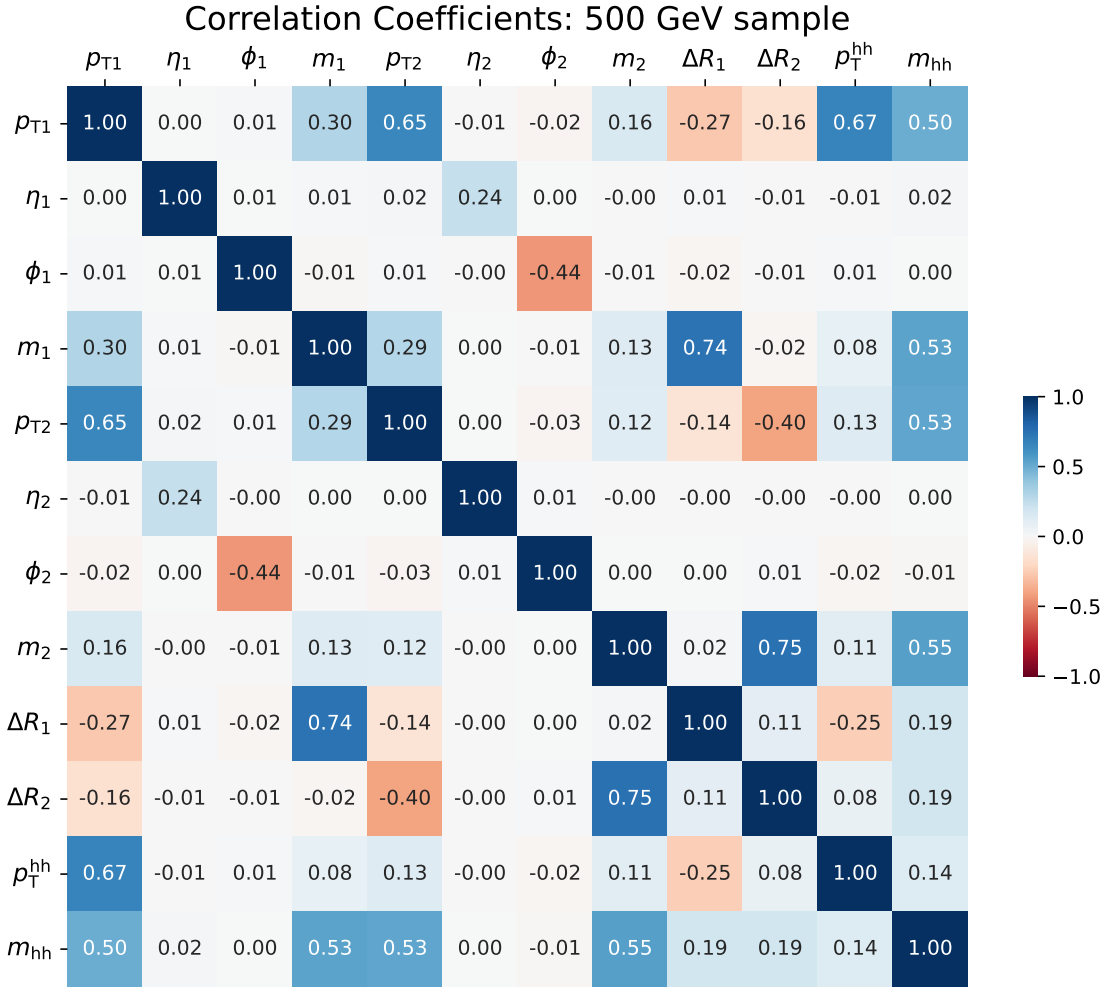

Figure 5: The correlation coefficients among different variables, which are computed from 500 GeV testing sample, which consists of 5k signal and 5k background.

The results show that the transverse momentum p_{T} and the invariant mass m of Higgs candidates are highly correlated to the total invariant mass. Figure 7 shows the scatter plots of the transverse momentum of the leading Higgs candidate and the total invariant mass m_{hh}. These plots also explain why the DNN only trained on background samples can also distinguish the signal and background events, because the background distribution in the signal and sideband regions are different.

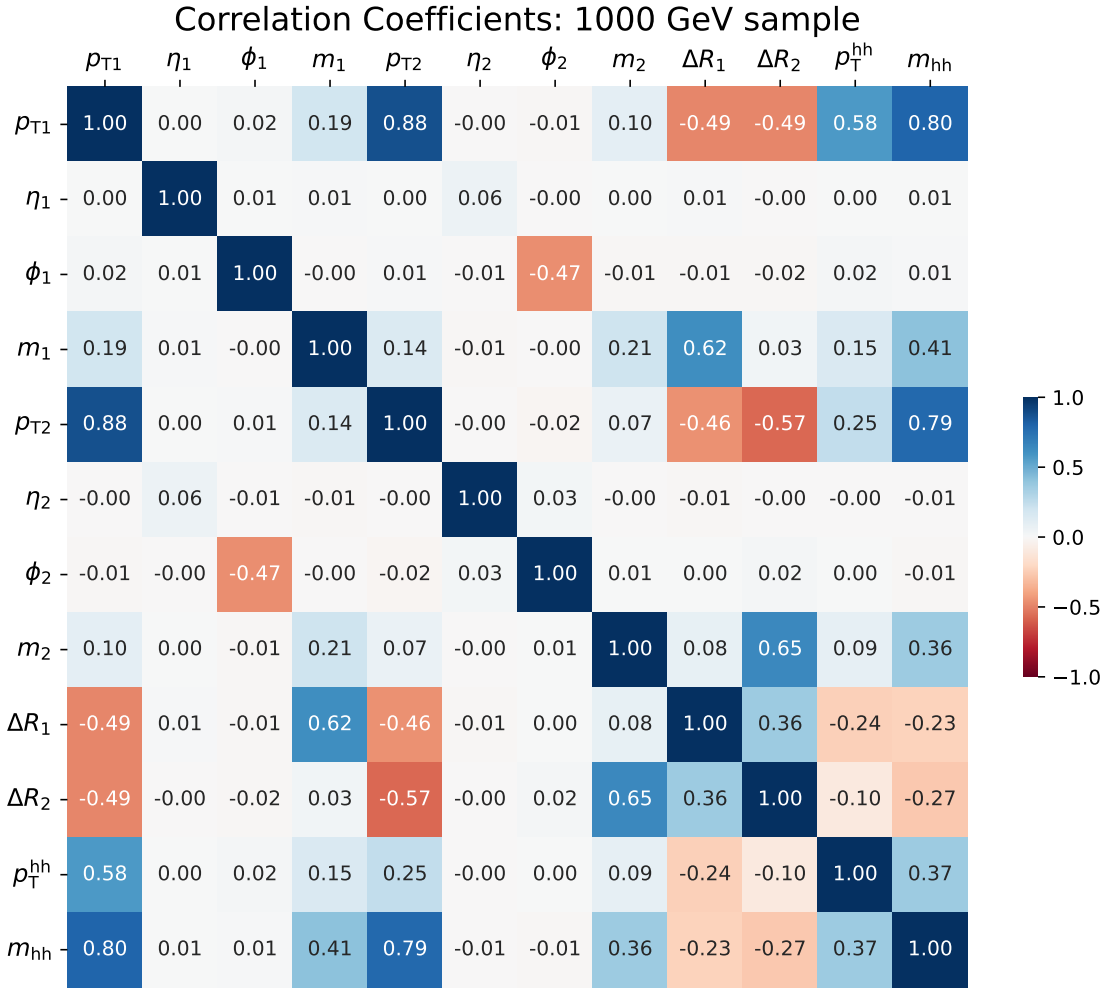

Figure 6: The correlation coefficients among different variables, which are computed from 1000 GeV testing sample, which consists of 5k signal and 5k background.

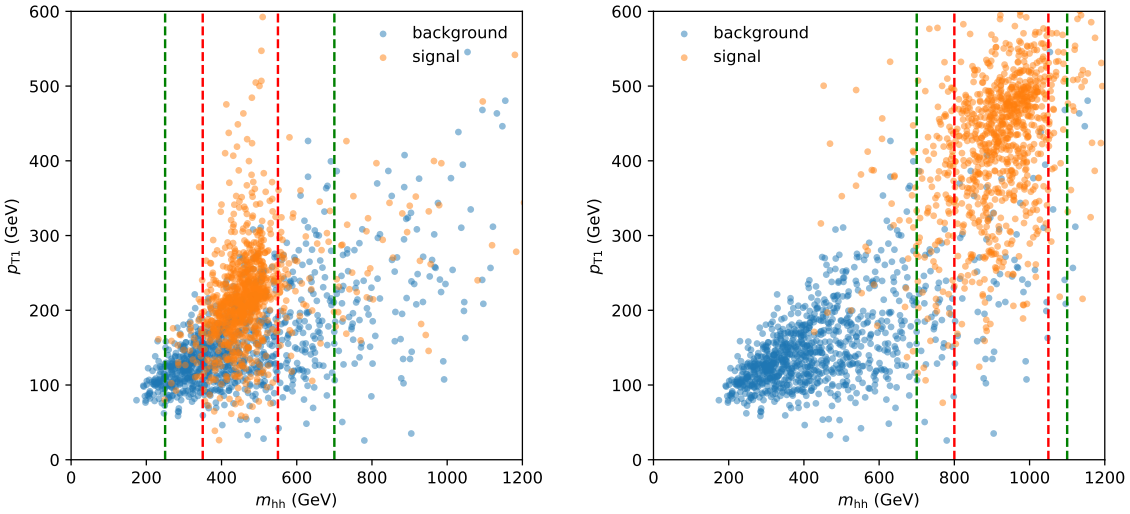

(a) $m_H = 500$ GeV (b) $m_H = 1000$ GeV

Figure 7: The scatter plots of the transverse momentum of leading Higgs candidate p_{T1} and total invariant mass m_{hh} distribution. The signal region is between the red dashed lines. The sideband region is between the green dashed lines and excludes the signal region.

2.4 Remove highly correlated features

Figure 5 and 6 show that the transverse momentum p_T and the invariant mass m of Higgs candidates are highly related to the total invariant mass m_{hh}. To investigate the impact of these highly correlated features on the discrimination power of CWoLa DNN models, we remove these input features and train the DNN model again.

Table 6: The CWoLa DNN training results. The transverse momentum and invariant mass of Higgs candidates are removed from samples. ACC is the best accuracy and AUC is the area under the ROC curve. The average and standard deviation of 10 training are presented.

m_H (GeV)		ACC	AUC
500	With signal	0.526 ± 0.020	0.536 ± 0.053
	No signal	0.532 ± 0.015	0.543 ± 0.029
1000	With signal	0.586 ± 0.030	0.625 ± 0.046
	No signal	0.564 ± 0.024	0.583 ± 0.042

Table 6 summarizes the results of the CWoLa DNN training without p_T and m features. The training datasets with and without signal events still have similar results. Compared to the previous one (Table 5) the accuracy values are closer to 0.5. These results suggest that

the removed features have a significant contribution to the model's discrimination power, and the remaining parameters are hard to utilize to distinguish the signal and background events.

2.5 Transverse momentum cut testing

In Figure 3, the distribution of the background sample exhibits a gradual termination around 150 GeV. To investigate whether this termination is a result of the "four-tag cut", which requires $p_{\mathrm{T}} > 40$ GeV, total invariant mass distributions with different p_{T} cuts are plotted in Figure 8. As the transverse momentum requirement increases from 40 GeV to 70 GeV, the termination point also shifts to larger values. Moreover, the termination remains gradual rather than an abrupt cut-off, suggesting that the gradual termination indeed results from the transverse momentum cut.

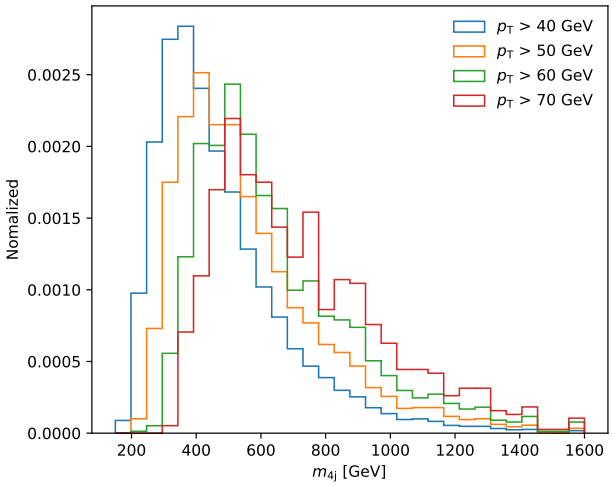

Figure 8: The total invariant mass $m_{4\mathrm{j}}$ distribution of background samples. The transverse momentum requirement is varied from 40 GeV to 70 GeV.

2.6 Enlarge the signal sample size

Another issue arises from the low signal fraction (Table 4), making DNN difficult to extract meaningful information about signal events. To investigate the impact of signal sample size, we increase the signal size manually and retrain the DNN model. The training sample sizes are summarized in Table 7.

Table 8 provides the results of the CWoLa DNN training without p_{T} and m features. For the 500 GeV case, the "0 times,", "1 times," and "10 times" samples yield similar results,

Table 7: The training sample size for the mixed sample. Various signal sizes are considered, and the background sizes are fixed for all cases. "1 times" represents the previous "With signal" case and "0 times" represents the previous "No signal" case.

		Signal				Background
m_H (GeV)	Mixed sample	1 times	0 times	10 times	100 times	All
500	M_1	244	0	2438	24380	200k
	M_2	28	0	276	2760	184k
1000	M_1	5	0	49	492	26k
	M_2	1	0	8	75	25k

Table 8: The CWoLa DNN training results. The transverse momentum and invariant mass of Higgs candidates are removed from samples. 1 time and 0 times are the with signal and no signal case in Table 6. ACC is the best accuracy and AUC is the area under the ROC curve. The average and standard deviation of 10 training are presented.

m_H (GeV)	times	ACC	AUC
500	1	0.526 ± 0.020	0.536 ± 0.053
	10	0.531 ± 0.027	0.533 ± 0.045
	100	0.634 ± 0.014	0.751 ± 0.030
	0	0.532 ± 0.015	0.543 ± 0.029
1000	1	0.586 ± 0.030	0.625 ± 0.046
	10	0.626 ± 0.027	0.678 ± 0.040
	100	0.621 ± 0.012	0.670 ± 0.023
	0	0.564 ± 0.024	0.583 ± 0.042

while "100 times" sample exhibits better performance. This suggests that the CWoLa DNN can extract meaningful information from the "100 times" sample. In the case of 1000 GeV, we can obtain better results when the signal sample size increases. The performance of 10 times and 100 times is similar. It seems that the training performance is saturated.

To further understand the behavior between 10 times and 100 times samples for the 500 GeV case, additional samples within this size range are generated, and the DNN is trained on these samples.

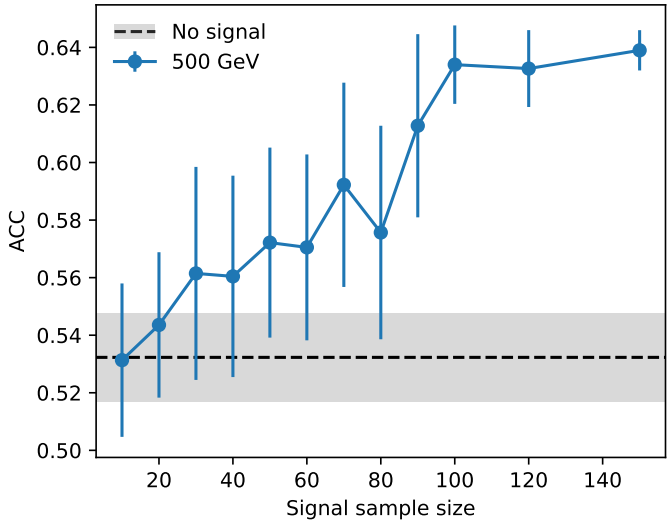

Figure 9: The accuracy of CWoLa DNN training as a function of the signal size. The unit of sample size is the size of the "1 times" case. The error bar is the standard deviation of 10 training. The grey band is the error bar of the "without signal" case.

Figure 9 is the training performance against the signal sample size. In this region, the performance increases when the signal size is increased. 120 times and 150 times samples are also generated and used in training. The accuracy is saturated at around 63%.

Similarly, for the 1000 GeV case, the DNN is trained on samples with sizes ranging from 1 to 10 times. Figure 10 is the training performance against the signal sample size. The performance is similar for all cases. The training accuracy is saturated at around 62%.

3 Physical data augmentation

The physical augmentations are inspired by Reference [2], which considers the rotation and smearing augmentations. These augmentations reflect both the symmetries in the physical event and the experimental resolution of the detector.

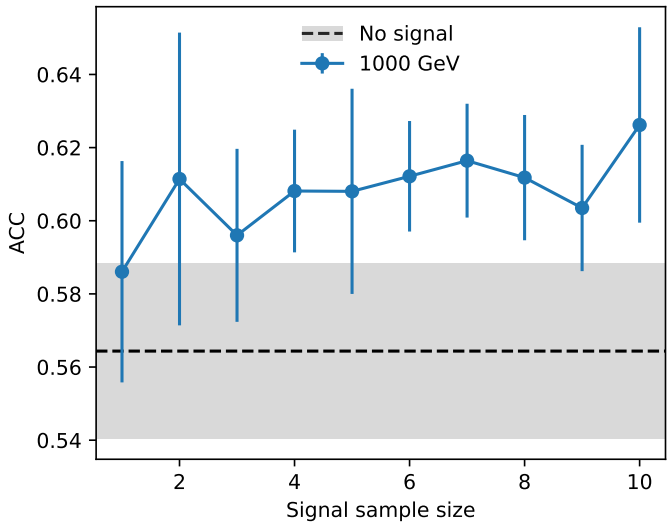

Figure 10: The performance of CWoLa DNN training as a function of the signal size. The unit of sample size is the size of the "1 times" case. The error bar is the standard deviation of 10 times training. The grey band is the error bar of the "without signal" case.

3.1 Original training data

The signal is the resonant Higgs boson pairs production in the four-b quarks channel. In this section, the Higgs boson pair is produced by the heavy CP-even scalar H with mass $m_H = 500$ GeV. The background consists of QCD multi-jet events. The basic requirement is the "four-tag cut," which requires at least four b-tagged $R = 0.4$ anti-k_t jets with $p_{\mathrm{T}} > 40$ GeV and $|\eta| < 2.5$. Only the events passing the four-tag cut are used in the following analysis.

The training samples consist of 50k signal events and 50k background events and the testing samples consist of 5k signal events and 5k background events.

The Higgs candidates are reconstructed by the min-ΔR pairing method. The input features are similar to the previous case (Table 1), but the b-tagging information is excluded.

3.2 Physical augmentation

We consider three different physical augmentations.

1. Azimuthal rotation: The final state is rotated by an angle ϕ randomly sampled from $[0, 2\pi]$.

2. $\eta - \phi$ smearing: The (η, ϕ) coordinate of Higgs candidates are resampled according to a Normal distribution centered on the original coordinate and with a standard deviation

inversely proportional to the p_{T}

$$\eta' \sim \mathcal{N}\left(\eta, \frac{\Lambda}{p_{\mathrm{T}}}\right), \quad \phi' \sim \mathcal{N}\left(\phi, \frac{\Lambda}{p_{\mathrm{T}}}\right) \tag{2}$$

where η', ϕ' are the augmented coordinate, p_{T} is the transverse momentum of the Higgs candidate, and the smearing scale is set to be $\Lambda = 10$ GeV.

3. p_{T} smearing: The p_{T} of Higgs candidates are resampled according to

$$p'_{\mathrm{T}} \sim \mathcal{N}\left(p_{\mathrm{T}}, f(p_{\mathrm{T}})\right), \quad f(p_{\mathrm{T}}) = \sqrt{0.052 p_{\mathrm{T}}^2 + 1.502 p_{\mathrm{T}}} \tag{3}$$

where p'_{T} is the augmented transverse momentum, $f\left(p_{\mathrm{T}}\right)$ is the energy smearing applied by `Delphes` (the p_{T}'s are normalised by 1 GeV).

Figure 11, 12 and 13 are the distributions before and after the augmentation. For the $\eta - \phi$ smearing, the distributions are similar for both cases. For p_{T} smearing, the peak broadens and the transverse momentum distribution looks smoother.

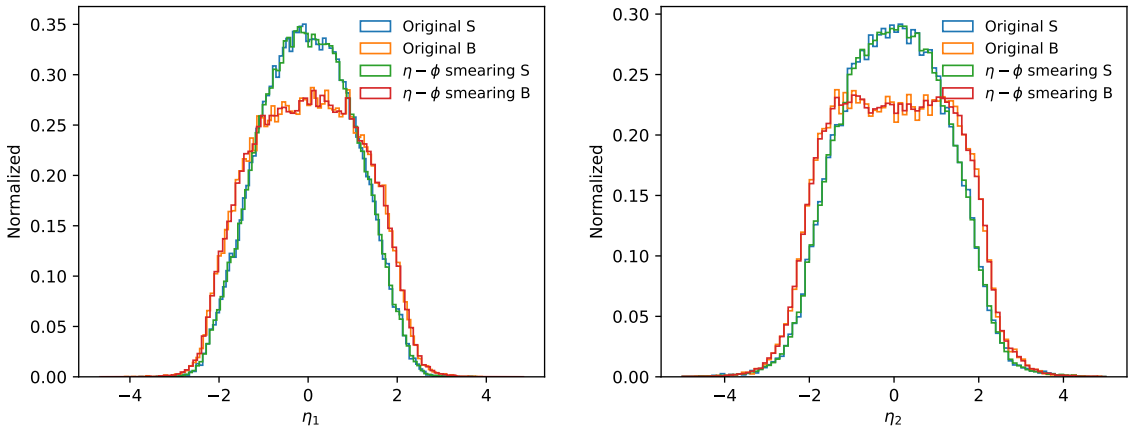

(a) Leading Higgs

(b) Sub-leading Higgs

Figure 11: The pseudorapidity distribution before and after the $\eta - \phi$ smearing augmentation. η_1 and η_2 are the pseudorapidities of the leading and the sub-leading Higgs candidate, respectively.

For each type of augmentation, we test "n times augmentation" with different n. The n times augmentation means for one original sample, we generate n augmented samples. Additionally, we test another case that applies all augmentations at the same time.

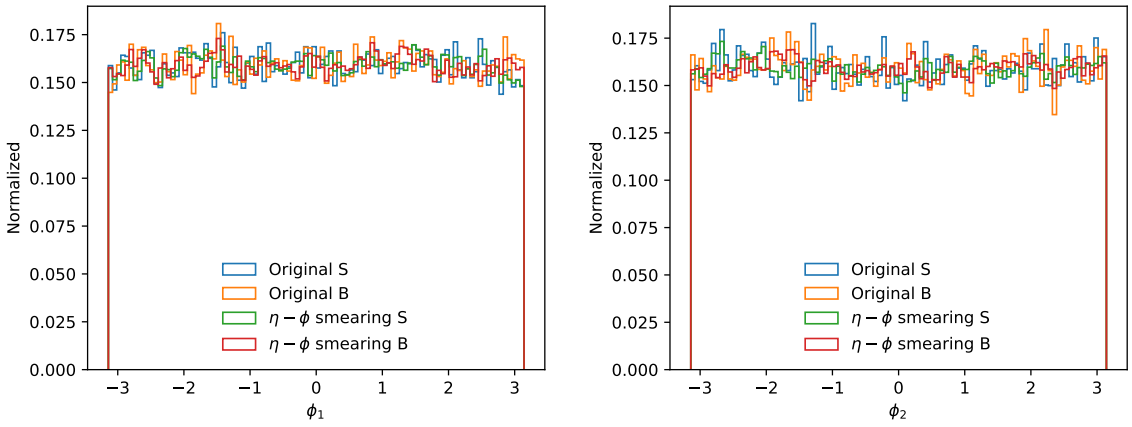

(a) Leading Higgs (b) Sub-leading Higgs

Figure 12: The azimuthal angle distribution before and after the $\eta - \phi$ smearing augmentation. ϕ_1 and ϕ_2 are the azimuthal angles of the leading and the sub-leading Higgs candidate, respectively.

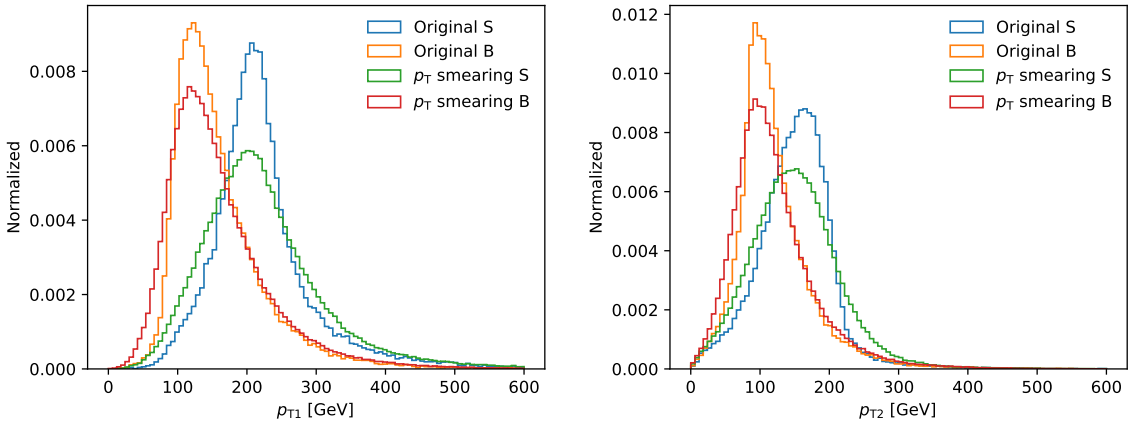

(a) Leading Higgs (b) Sub-leading Higgs

Figure 13: The transverse momentum distribution before and after the p_T smearing augmentation. p_{T1} and p_{T2} are the transverse momentum of the leading and the sub-leading Higgs candidates, respectively.

3.3 Training results

Table 9 presents the DNN classification training results of the original sample. Table 10 are the training results of the augmented samples. For each type of augmentation, they all can improve the ACC by about 4%. The differences among the various augmentation are not significant. The 10-times augmentation has the best results, but the difference between the 5-times and 10-times augmentation is tiny. It seems that the performance of this classifier is saturated.

Table 9: The training results of original samples. ACC is the best accuracy and AUC is the area under the ROC curve. The average and standard deviation of 10 training are presented.

	Original
ACC	0.845 ± 0.015
AUC	0.917 ± 0.005

Table 10: The training results of augmented samples. "+ 3 times" means the training sample consists of the original sample and 3 times the augmented sample. ACC is the best accuracy and AUC is the area under the ROC curve. The average and standard deviation of 10 training are presented.

Sample		Rotation	$\eta - \phi$ smear	p_{T} smear	All
+ 3 times	ACC	0.880 ± 0.007	0.879 ± 0.010	0.882 ± 0.003	0.875 ± 0.011
	AUC	0.950 ± 0.007	0.949 ± 0.008	0.951 ± 0.003	0.942 ± 0.012
+ 5 times	ACC	0.887 ± 0.002	0.887 ± 0.001	0.890 ± 0.002	0.889 ± 0.003
	AUC	0.955 ± 0.001	0.955 ± 0.001	0.957 ± 0.001	0.956 ± 0.001
+ 10 times	ACC	0.889 ± 0.001	0.889 ± 0.002	0.892 ± 0.002	0.892 ± 0.002
	AUC	0.956 ± 0.001	0.956 ± 0.001	0.958 ± 0.001	0.958 ± 0.000

3.4 Deeper model

In Section 3.3, the DNN model consists of 2 hidden layers, each containing 64 hidden nodes. To explore the impact of the model structure, the deeper DNN model is trained. We investigate the performance of the DNN model with 5 hidden layers.

Table 11 are the training results with a deeper DNN model. Models are only trained on the "All augmentation" sample because from Table 10 we found that four augmentation methods yielded similar results. The results show that the augmented sample can improve

Table 11: The training results of deeper DNN model. "+ 3 times" means the training sample consists of the original sample and 3 times the augmented sample. ACC is the best accuracy and AUC is the area under the ROC curve. The average and standard deviation of 10 training are presented.

Sample		Original	+ 3 times	+ 5 times	+ 10 times
All augmentation	ACC	0.864 ± 0.005	0.890 ± 0.002	0.890 ± 0.002	0.884 ± 0.005
	AUC	0.928 ± 0.005	0.957 ± 0.001	0.957 ± 0.001	0.949 ± 0.005

ACC to 89%, even from the "+ 3 times" case and this accuracy value is similar to the previous test. These findings suggest that the classifier may have reached a saturation point and point out the difficulty of further improving accuracy on this test sample.

4 Hidden valley model

4.1 Sample generation

The signal process is $f\overline{f} \to Z_V$, where Z_V is the massive gauge boson linking SM and the dark sector. The hidden Z_V boson would decay to a pair of dark quark $q_V\overline{q}_V$, which would lead to two jets in the detector. The signal sample is generated by `Pythia` and the detector simulation is done by `Delphes`. For jet reconstruction, the anti-k_t algorithm is utilized with parameter $R = 0.8$.

The background sample is the SM di-jet sample. This process is generated at $\sqrt{s} =$ 13 TeV. Following are the `MadGraph` scripts for generating background samples:

```
generate p p > j j
output ppjj
launch ppjj

shower=Pythia8
detector=Delphes
analysis=OFF
madspin=OFF
done

Cards/delphes_card_CMS.dat
```

```
set run_card nevents 10000
set run_card ebeam1 6500.0
set run_card ebeam2 6500.0

set run_card ptj 700
set run_card etaj 2.2
set run_card mmjj 3000

done
```

4.2 Problem for generating signal sample

Error messages:

```
PYTHIA Error: input string not found in settings databases::
  HiddenValley:separateFlav    = on      ! Consider different flavours

PYTHIA Error: input particle not found in Particle Data Table:
  4900102:m0                   = 10.3306

...
```

Solution: This problem arises from the `Pythia` version. At first, `Pythia 8.306` is used to generate signal samples. Some features are not included in this version. We should use `Pythia 8.307` at least. More details between 8.306 and 8.307 can be found in this page.

4.3 Sample selection

The selection cuts after the `Delphes` simulation:

- n_j cut: The number of jets should be greater than or equal to 2.
- p_{T} cut: The transverse momentum of two highest p_{T} jets should greater 750 GeV.
- η cut: The η range of two highest p_{T} jets are require $|\eta| < 2$.
- Signal region: Total invariant mass of two leading jets m_{jj} belonging to $[4700, 5500]$.
- Sideband region: Total invariant mass of two leading jets m_{jj} belonging to $[4300, 4700] \cup [5500, 5900]$.

Table 12 is the cutflow number at different selection cuts. Figure 14 is transverse momentum distribution after n_j cut. Figure 15 is the m_{jj} distribution after the η cut.

Table 12: The number of passing events and passing rates for signal and background processes at different selection cuts.

Cut	Signal	pass rate	Background	pass rate
Total	10000	1	100000	1
n_j cut	10000	1.00	99963	1.00
p_{T} cut	9890	0.99	57832	0.58
η cut	8975	0.90	55523	0.56
SR region	5497	0.55	1991	0.02
SB region	1667	0.17	3090	0.03

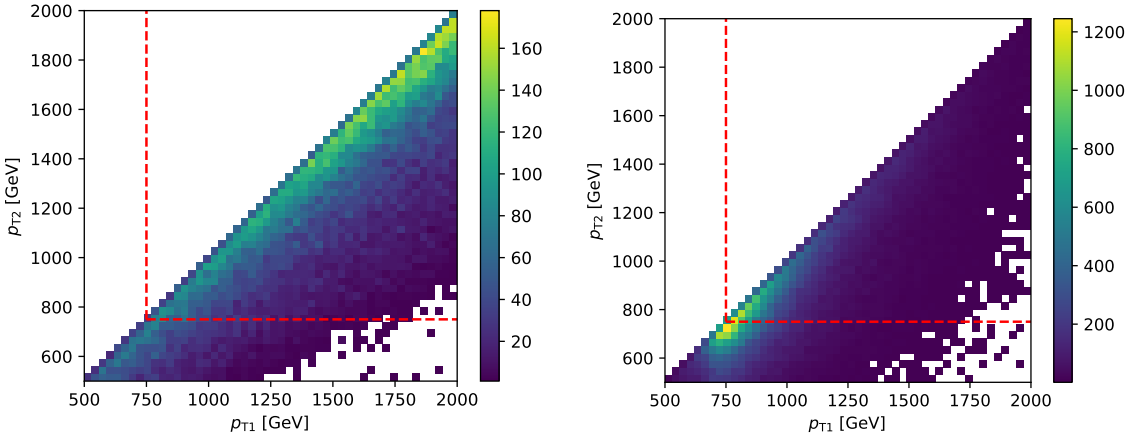

(a) Signal

(b) Background

Figure 14: The transverse momentum distribution of leading and sub-leading jets. The red dashed lines are the p_{T} cut.

References

[1] Jack H. Collins, Kiel Howe, and Benjamin Nachman. Anomaly Detection for Resonant New Physics with Machine Learning. *Phys. Rev. Lett.*, 121(24):241803, 2018.

[2] Barry M. Dillon, Luigi Favaro, Friedrich Feiden, Tanmoy Modak, and Tilman Plehn. Anomalies, Representations, and Self-Supervision. 1 2023.

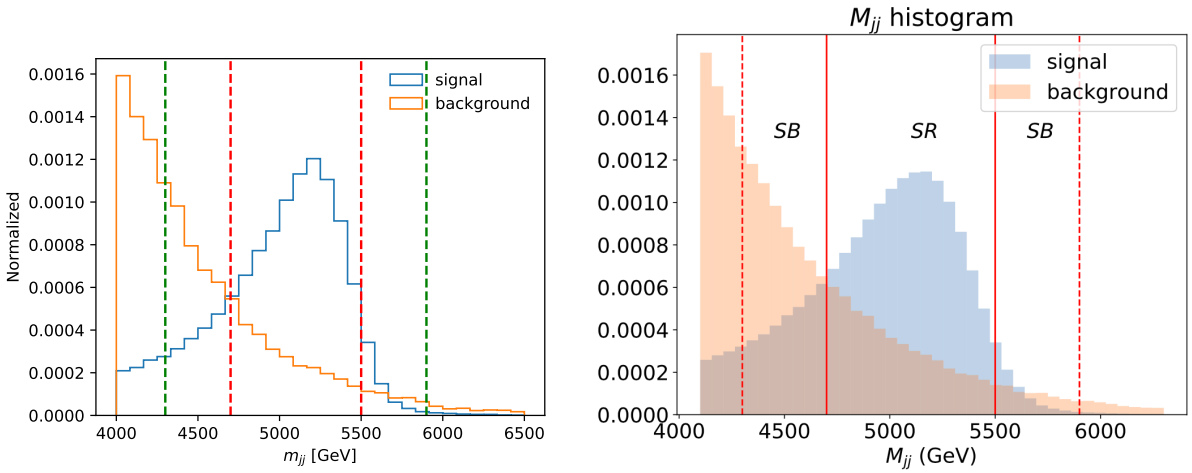

(a) My plot

(b) Zong-En's plot

Figure 15: The totoal invriant mass m_{jj} distribution of signal and background samples. In my plot, the signal region is between the red dashed lines. The sideband region is between the green dashed lines and excludes the signal region.